YALE PEABODY MUSEUM

JOURNAL OF MARINE RESEARCH

The *Journal of Marine Research,* one of the oldest journals in American marine science, published important peer-reviewed original research on a broad array of topics in physical, biological, and chemical oceanography vital to the academic oceanographic community in the long and rich tradition of the Sears Foundation for Marine Research at Yale University.

An archive of all issues from 1937 to 2021 (Volume 1–79) are available through EliScholar, a digital platform for scholarly publishing provided by Yale University Library at https://elischolar.library.yale.edu/.

Requests for permission to clear rights for use of this content should be directed to the authors, their estates, or other representatives. The *Journal of Marine Research* has no contact information beyond the affiliations listed in the published articles. We ask that you provide attribution to the *Journal of Marine Research.*

Yale University provides access to these materials for educational and research purposes only. Copyright or other proprietary rights to content contained in this document may be held by individuals or entities other than, or in addition to, Yale University. You are solely responsible for determining the ownership of the copyright, and for obtaining permission for your intended use. Yale University makes no warranty that your distribution, reproduction, or other use of these materials will not infringe the rights of third parties.

Numerical solution of the two-layer shallow water equations with bottom topography

by Rick Salmon[1]

ABSTRACT

We present a simple, robust numerical method for solving the two-layer shallow water equations with arbitrary bottom topography. Using the technique of operator splitting, we write the equations as a pair of hyperbolic systems with readily computed characteristics, and apply third-order-upwind differences to the resulting wave equations. To prevent the thickness of either layer from vanishing, we modify the dynamics, inserting an artificial form of potential energy that becomes very large as the layer becomes very thin. Compared to high-order Riemann schemes with flux or slope limiters, our method is formally more accurate, probably less dissipative, and certainly more efficient. However, because we do not exactly conserve momentum and mass, bores move at the wrong speed unless we add explicit, momentum-conserving viscosity. Numerical solutions demonstrate the accuracy and stability of the method. Solutions corresponding to two-layer, wind-driven ocean flow require no explicit viscosity or hyperviscosity of any kind; the implicit hyperdiffusion associated with third-order-upwind differencing effectively absorbs the enstrophy cascade to small scales.

1. Introduction

This paper offers a simple, robust, numerical method for solving the two-layer shallow water equations with arbitrary bottom topography. Either layer thickness, and hence the total fluid depth, may be arbitrarily small. Our strategy is to use the technique of operator splitting to rewrite the two-layer equations as a *pair* of hyperbolic systems. In characteristic form, each equation describes propagation at a unique velocity. We solve these equations by the method of third-order-upwind differences, with the upwind direction based upon the unique propagation direction in each equation.

Like the shallow water equations themselves, these finite-difference equations become unstable if either layer thickness vanishes. To prevent this, we modify the dynamics, inserting an artificial form of potential energy that becomes very large as the layer becomes very thin. This modification prevents the layer thicknesses from falling below an arbitrarily small (and therefore dynamically insignificant) lower bound. Thus, in the case of no forcing, the two-layer model relaxes to a state of rest in which the interface between the

---

1. Scripps Institution of Oceanography, University of California, 9500 Gilman Drive, La Jolla, California, 92093-0213, U.S.A. *email: rsalmon@ucsd.edu*

layers is flat, *except* in shallow regions, where the lower layer is present as a thin film beneath an upper layer of much greater thickness.

The most sophisticated numerical methods for solving systems of equations like the shallow water equations are based upon high-order, conservative, Riemann solvers.[2] Unfortunately, these methods place a very high demand on computing resources. The methods presented here arose in the search for an efficient, two-layer, numerical ocean circulation model that could be integrated for the decades of simulated time required to reach equilibrium, despite the short time steps imposed by the presence of fast external gravity waves. Such simulations require millions of time steps, and efficiency therefore demands a simple algorithm. However, the algorithm must accommodate the vanishing of either layer thickness, and it must not require an excessive friction or eddy dissipation for stability. The satisfaction of all these requirements poses a considerable challenge.

Although the ideas involved are quite simple, they are most easily explained by considering progressively more complicated cases. Section 2 explains the upwind-differencing method by applying it to the one-layer shallow water equations *without* bottom topography. Section 3 uses the technique of operator splitting to extend the method to the two-layer case. In Section 4 we add bottom topography to the one-layer model, employing the artificial potential to prevent the layer thickness from vanishing. Section 5 derives the complete two-layer model with topography. Section 6 presents some numerical solutions that demonstrate the accuracy and stability of the method. We find that solutions corresponding to two-layer, wind-driven ocean flow require no explicit viscosity or hyperviscosity of any kind; the implicit hyperdiffusion associated with third-order-upwind differencing is by itself sufficient to prevent enstrophy from accumulating at the smallest resolved scales. Section 7 summarizes the paper.

2. The one-layer case

First consider the one-layer shallow water equations without bottom topography. In one space dimension, these equations may be written in the form

$$\frac{\partial}{\partial t}(u + 2c) + (u + c)\frac{\partial}{\partial x}(u + 2c) = 0 \qquad (2.1a)$$

and

$$\frac{\partial}{\partial t}(u - 2c) + (u - c)\frac{\partial}{\partial x}(u - 2c) = 0 \qquad (2.1b)$$

Here $u(x, t)$ is the velocity at location x and time t of the fluid layer with thickness $h(x, t)$, g is the gravity constant, and $c \equiv \sqrt{gh}$. The quantities $u \pm 2c$ are Riemann invariants. Each of (2.1) takes the form

---

2. For an excellent introduction to these methods, see LeVeque (1992) or Godlewski and Raviart (1996). For a more basic but more specific survey of numerical methods applied to the shallow water equations, see Vreugdenhil (1994).

$$\frac{\partial \theta}{\partial t} + U \frac{\partial \theta}{\partial x} = 0 \tag{2.2}$$

of a one-dimensional advection equation. To solve (2.2) we replace the x-derivative by the third-order-upwind approximation,

$$U \frac{\partial \theta}{\partial x} = \begin{cases} \dfrac{U}{6\Delta} (\theta_{i-2} - 6\theta_{i-1} + 3\theta_i + 2\theta_{i+1}) \equiv U\vec{\theta}_x, & U > 0 \\[2ex] \dfrac{U}{6\Delta} (-2\theta_{i-1} - 3\theta_i + 6\theta_{i+1} - \theta_{i+2}) \equiv U\overleftarrow{\theta}_x, & U < 0 \end{cases} \tag{2.3}$$

In (2.3) Δ is the grid spacing, and θ_i is the value of θ at the i-th gridpoint. Both $\vec{\theta}_x$ and $\overleftarrow{\theta}_x$ are logical finite-difference approximations to $\partial\theta/\partial x$. The arrows connote the direction of U. By the usual Taylor-series expansions, (2.2) with (2.3) implies

$$\frac{\partial \theta}{\partial t} + U \frac{\partial \theta}{\partial x} = -\frac{|U|}{12} \Delta^3 \theta_{xxxx} + O(\Delta^4). \tag{2.4}$$

Thus the truncation error of scheme (2.3) takes the form of hyper-diffusion, with diffusion coefficient $|U|\Delta^3/12$. Assuming $|u| < c$, the corresponding approximations to (2.1) are equivalent to

$$u_t + uu_x + gh_x = -\frac{\Delta^3}{12} [cu_{xxxx} + 2uc_{xxxx}] \tag{2.5a}$$

and

$$h_t + (hu)_x = -\frac{\Delta^3}{12} \left[\frac{hu}{c} u_{xxxx} + 2hc_{xxxx} \right] \tag{2.5b}$$

in which the truncation error corresponds to hyperdiffusion of mass as well as momentum; neither is exactly conserved. In addition (2.5) contain cross-diffusion terms—the c_{xxxx}-term in (2.5a) and the u_{xxxx}-term in (2.5b)—but these are relatively small if $|u| \ll c \equiv \sqrt{gh}$. Neither the cross-diffusion terms nor, probably, the hyperdiffusion of mass would occur in the more typical scheme in which an explicit biharmonic eddy diffusivity is intentionally put into the equations.

The case for third-order upwinding has been made by Leonard (1984); see also Leonard (1979, 1991). Briefly, even-order-accurate approximations to $\partial\theta/\partial x$ correspond to oscillatory truncation error that causes grid-mode oscillations—wiggles—in numerical solutions. On the other hand, odd-order schemes are either absolutely stable (upwind schemes) or absolutely unstable (downwind schemes). The best known method for solving (2.1)—Godunov's method—is based upon the *first*-order-upwind approximation to $U\partial\theta/\partial x$. However, Godunov's method is notoriously diffusive; the analogue of (2.4) contains *normal* diffusion with a coefficient of order $|U|\Delta$. The significant advantage of (2.3) is its higher-order (i.e. more scale-selective) diffusion. Third-order upwinding seems especially

appealing because its truncation error corresponds to biharmonic diffusion of the type often inserted explicitly, at an additional cost in computations. In a study of passive tracer advection, Hecht *et al.* (1995) have shown that third-order upwinding compares favorably to other popular sub-gridscale dissipation schemes.

Note that we postpone replacing $\partial/\partial t$ by a finite-difference approximation; the *semi-discrete* equations (2.4) and (2.5) retain analytic time derivatives. The resulting freedom to choose the time step independently from the space discretization will prove to be important. Moreover, Kurganov and Tadmor (2000) show that schemes that mix the space- and time-discretization, including some schemes widely used for hyperbolic systems, have a truncation error that blows up as the time step is decreased.

In two dimensions, the one-layer shallow water equations,

$$\frac{\partial u}{\partial t} + u \frac{\partial u}{\partial x} + v \frac{\partial u}{\partial y} = -2c \frac{\partial c}{\partial x} \tag{2.6a}$$

$$\frac{\partial v}{\partial t} + u \frac{\partial v}{\partial x} + v \frac{\partial v}{\partial y} = -2c \frac{\partial c}{\partial y} \tag{2.6b}$$

$$\frac{\partial c}{\partial t} + u \frac{\partial c}{\partial x} + v \frac{\partial c}{\partial y} = -\frac{1}{2} c \left(\frac{\partial u}{\partial x} + \frac{\partial v}{\partial y} \right) \tag{2.6c}$$

cannot be written in a form analogous to (2.2). Instead, we use (2.6a) and (2.6c) to write

$$\frac{\partial}{\partial t} (u + 2c) + (u + c) \frac{\partial}{\partial x} (u + 2c) + v \frac{\partial}{\partial y} (u + 2c) + c \frac{\partial v}{\partial y} = 0 \tag{2.7a}$$

and

$$\frac{\partial}{\partial t} (u - 2c) + (u - c) \frac{\partial}{\partial x} (u - 2c) + v \frac{\partial}{\partial y} (u - 2c) - c \frac{\partial v}{\partial y} = 0 \tag{2.7b}$$

The equations (2.7) fit the two-dimensional advection form,

$$\frac{\partial \theta}{\partial t} + U \frac{\partial \theta}{\partial x} + V \frac{\partial \theta}{\partial y} = 0 \tag{2.8}$$

with $\theta = u \pm 2c$, $U = u \pm c$, and $V = v$, *except* for the $\pm c \partial v/\partial y$-terms at the end of each equation. However, we shall use (2.7) only to compute $\partial u/\partial t$ and the *contribution* to $\partial c/\partial t$ from the *x*-derivative terms in (2.6c). (We obtain $\partial v/\partial t$ and the contribution of the *y*-derivative terms to $\partial c/\partial t$ by the analogous treatment of (2.6b) and (2.6c).) $\partial u/\partial t$ is obtained by adding (2.7a) and (2.7b), but the $\pm c \partial v/\partial y$-terms then cancel. $\partial c/\partial t$ is obtained by subtracting (2.7b) from (2.7a), but the $\pm c \partial v/\partial y$-terms do not contribute to the sought-for *x*-derivative-terms. Thus we may proceed by *ignoring* the last terms in (2.7), and by treating the remaining terms as we did in the case of (2.2–3). That is, we approximate

$$A = -(u + c)(u + 2c)_x \qquad C = -v(u + 2c)_y$$
$$B = -(u - c)(u - 2c)_x \qquad D = -v(u - 2c)_y \qquad (2.9)$$

using the obvious generalization of (2.3). For example,

$$C = \begin{cases} -v\vec{\theta}_y, & v > 0 \\ -v\tilde{\theta}_y, & v < 0 \end{cases} \qquad \text{with} \qquad \theta = u + 2c, \qquad (2.10)$$

while the formula for B depends upon the sign of $u - c$. Here, as in (2.3),

$$\vec{\theta}_y \equiv \frac{1}{6\Delta} (\theta_{i,j-2} - 6\theta_{i,j-1} + 3\theta_{i,j} + 2\theta_{i,j+1}) \qquad (2.11)$$

denotes the third-order-upwind estimate of $\partial\theta/\partial y$, with the "wind" blowing toward positive y. Similarly,

$$\tilde{\theta}_y \equiv \frac{1}{6\Delta} (-2\theta_{i,j-1} - 3\theta_{i,j} + 6\theta_{i,j+1} - \theta_{i,j+2}). \qquad (2.12)$$

Then, solving (2.7) for the time-derivative terms, we obtain

$$\frac{\partial u}{\partial t} = \frac{1}{2} (A + B + C + D) \qquad (2.13)$$

and

$$\frac{\partial}{\partial t} \sqrt{gh} = \frac{1}{4} (A - B) + \cdots \qquad (2.14)$$

In (2.14) we omit the terms proportional to C and D. These terms—and the already ignored $\pm c \partial v/\partial y$-terms in (2.7)—contribute to the y-derivative terms in the continuity equation, but for the moment we only want the x-derivative terms. That is, (2.13) and the terms explicitly appearing in (2.14) are logical finite-difference approximations to (2.6a) and

$$\frac{\partial h}{\partial t} = -\frac{\partial(hu)}{\partial x}, \qquad (2.15)$$

respectively.

We obtain the analogous expression for $\partial v/\partial t$ and the additional term needed in (2.14) by repeating the entire procedure in the y-direction, that is, by manipulating (2.6b) and (2.6c) in a manner analogous to the manipulations just performed on (2.6a) and (2.6c). The results analogous to (2.13) and (2.14) are

$$\frac{\partial v}{\partial t} = \frac{1}{2} (E + F + G + J) \qquad (2.16)$$

and

$$\frac{\partial}{\partial t}\,\sqrt{gh} = \frac{1}{4}\,(E - F) + \cdots \tag{2.17}$$

where

$$\begin{matrix} E = -(v + c)(v + 2c)_y & G = -u(v + 2c)_x \\ F = -(v - c)(v - 2c)_y & J = -u(v - 2c)_x \end{matrix} \tag{2.18}$$

are the analogues of (2.9). As in (2.9), we replace the derivatives in (2.18) by third-order-upwind approximations in the manner illustrated by (2.10–12). In this case, the terms appearing explicitly in (2.17) correspond to the y-derivative terms in the continuity equation. Then, combining (2.14) and (2.17), we obtain the finite-difference analogue,

$$\frac{\partial}{\partial t}\,\sqrt{gh} = \frac{1}{4}\,(A - B + E - F), \tag{2.19}$$

of (2.6c).

In overall summary, our finite-difference approximation to (2.6) is (2.13), (2.16), and (2.19) with the expressions (2.9) and (2.18) replaced by third-order-upwind approxima-tions. Once again, these equations are semi-discrete; we discuss the method for discretizing $\partial/\partial t$ in Section 5. We incorporate forcing terms not involving spatial derivatives by simply adding them to the right-hand sides of (2.13) or (2.16). For example, to add the Coriolis force, we append $+fv$ to (2.13) and $-fu$ to (2.16) (where f is the Coriolis parameter) with no change in the method used to calculate (2.9) and (2.18).

3. The two-layer case

Next we consider the two-layer shallow water equations,

$$\frac{\partial \mathbf{u}_1}{\partial t} + \mathbf{u}_1 \cdot \nabla \mathbf{u}_1 = -g\nabla(h_1 + h_2) \tag{3.1a}$$

$$\frac{\partial \mathbf{u}_2}{\partial t} + \mathbf{u}_2 \cdot \nabla \mathbf{u}_2 = -g(1 - \varepsilon)\nabla h_1 - g\nabla h_2 \tag{3.1b}$$

$$\frac{\partial h_1}{\partial t} + \nabla \cdot (h_1\mathbf{u}_1) = 0 \tag{3.1c}$$

$$\frac{\partial h_2}{\partial t} + \nabla \cdot (h_2\mathbf{u}_2) = 0. \tag{3.1d}$$

Here h_1 and $\mathbf{u}_1 = (u_1, v_1)$ are the thickness and velocity of the upper layer; h_2 and $\mathbf{u}_2$ are the corresponding variables in the lower layer; $\nabla \equiv (\partial_x, \partial_y)$; and ε is the relative density difference between the layers. Thus $g\varepsilon$ is the reduced gravity.

Quasi-linear systems like (3.1) with three or more independent variables are rarely hyperbolic.[3] However, if the one-dimensional form

$$\frac{\partial u_1}{\partial t} + u_1 \frac{\partial u_1}{\partial x} + g \frac{\partial h_1}{\partial x} + g \frac{\partial h_2}{\partial x} = 0$$

$$\frac{\partial u_2}{\partial t} + u_2 \frac{\partial u_2}{\partial x} + g(1 - \varepsilon) \frac{\partial h_1}{\partial x} + g \frac{\partial h_2}{\partial x} = 0$$

$$\frac{\partial h_1}{\partial t} + u_1 \frac{\partial h_1}{\partial x} + h_1 \frac{\partial u_1}{\partial x} = 0$$

$$\frac{\partial h_2}{\partial t} + u_2 \frac{\partial h_2}{\partial x} + h_2 \frac{\partial u_2}{\partial x} = 0$$

$$(3.2)$$

of (3.1) were hyperbolic, then we could apply our strategy separately in each direction, and combine the results, as we have done in Section 2.

We begin by recalling the definition of a hyperbolic system. (See, for example, LeVeque (1992).) The quasi-linear system

$$\frac{\partial u_i}{\partial t} + A_{ij} \frac{\partial u_j}{\partial x} = 0 \tag{3.3}$$

is hyperbolic if all the eigenvalues of matrix A are real, and all the left eigenvectors of A are distinct. Here, repeated subscripts are summed from 1 to n, the number of independent variables. That is, if

$$\alpha_i^k A_{ij} = c^k \alpha_j^k, \tag{3.4}$$

where c^k, satisfying

$$\det [A - cI] = 0, \tag{3.5}$$

is the k-th eigenvalue of A and α_i^k is the i-th component of the corresponding left eigenvector, then (3.3) may be written as n equations of the form

$$\alpha_i^k \left(\frac{\partial u_i}{\partial t} + c^k \frac{\partial u_i}{\partial x} \right) = 0, \tag{3.6}$$

in which all the dependent variables are advected with the same velocity c^k. For special α_i^k it may be possible to write (3.6) in the form (2.2). That is, Riemann invariants may exist. However, the general form (3.6) is all that is required to apply the third-order-upwind method.

Eq. (3.2) fits the form of (3.3) with $n = 4$ and $(u_1, u_2, u_3, u_4) = (u_1, u_2, h_1, h_2)$. Lawrence (1990) gives explicit formulae for the corresponding eigenvalues. As expected,

---

3. For a discussion of this point, see Whitham (1974), pp. 139–141.

these eigenvalues correspond to the phase speeds of external and internal gravity waves. However, if the internal Froude number

$$\frac{(u_1 - u_2)^2}{\varepsilon g(h_1 + h_2)} \tag{3.7}$$

exceeds a critical value (approximately equal to unity in the Boussinesq case, $\varepsilon \ll 1$), then the phase speed corresponding to internal gravity waves becomes imaginary, and the system ceases to be hyperbolic. Even if this never occurs, the calculation described by Lawrence, which amounts to finding the roots of a quartic polynomial that does not factorize, requires too much computation to be practical.

We overcome this difficulty by splitting (3.1) into two parts. The first part,

$$\frac{\partial \mathbf{u}_1}{\partial t} + \mathbf{u}_1 \cdot \nabla \mathbf{u}_1 = 0, \quad \frac{\partial \mathbf{u}_2}{\partial t} + \mathbf{u}_2 \cdot \nabla \mathbf{u}_2 = 0$$

$$\frac{\partial h_1}{\partial t} + \mathbf{u}_1 \cdot \nabla h_1 = 0, \quad \frac{\partial h_2}{\partial t} + \mathbf{u}_2 \cdot \nabla h_2 = 0 \tag{3.8}$$

contains only the advection terms in (3.1). The second part,

$$\frac{\partial \mathbf{u}_1}{\partial t} + g\nabla(h_1 + h_2) = 0, \quad \frac{\partial \mathbf{u}_2}{\partial t} + g(1 - \varepsilon)\nabla h_1 + g\nabla h_2 = 0$$

$$\frac{\partial h_1}{\partial t} + h_1\nabla \cdot \mathbf{u}_1 = 0, \qquad\qquad \frac{\partial h_2}{\partial t} + h_2\nabla \cdot \mathbf{u}_2 = 0 \tag{3.9}$$

contains everything else. Both parts may be rewritten in a form analogous to (3.6), and hence we may use third-order-upwind differences on both parts. Indeed, each of (3.8) already takes the form (2.8), to which we can apply the obvious generalization of (2.3). On the other hand, (3.9) requires the one-direction-at-a-time strategy of Section 2, and the general method outlined in (3.3–6). On physical grounds it is obvious that the one-dimensional form of (3.9), namely,

$$\frac{\partial u_1}{\partial t} + g\frac{\partial h_1}{\partial x} + g\frac{\partial h_2}{\partial x} = 0 \tag{3.10a}$$

$$\frac{\partial u_2}{\partial t} + g(1 - \varepsilon)\frac{\partial h_1}{\partial x} + g\frac{\partial h_2}{\partial x} = 0 \tag{3.10b}$$

$$\frac{\partial h_1}{\partial t} + h_1\frac{\partial u_1}{\partial x} = 0 \tag{3.10c}$$

$$\frac{\partial h_2}{\partial t} + h_2\frac{\partial u_2}{\partial x} = 0 \tag{3.10d}$$

is hyperbolic; since (3.10) corresponds to linearization of the dynamics about a state of rest, the corresponding wave speeds *must* be real.

Once the form (3.6) of (3.10) has been found, we solve (3.1) by alternately time-stepping (3.8) and (3.9). That is, each timestep of (3.8) is followed by a timestep of (3.9). This technique, called *operator splitting,* can be problematic when the physics involves a balance between terms occurring in different parts of the split. However, operator splitting succeeds for (3.8–9). Stone and Norman (1992) describe a similar splitting of advection from everything else in a two-dimensional magneto-hydrodynamics code.

For the two-layer system (3.10), the requirement (3.5) leads to

$$c = \pm c_e, \pm c_i \tag{3.11}$$

where c_e and c_i, given by

$$c_e^2, c_i^2 = \frac{1}{2}(gh_1 + gh_2) \pm \frac{1}{2}\{(gh_1 + gh_2)^2 - 4\varepsilon g h_1 g h_2\}^{1/2}, \tag{3.12}$$

are the external- and internal-gravity-wave speeds, respectively. For each c given by (3.11–12), we take $\alpha_1 = h_1$ and solve (3.4) for

$$\alpha_2 = \frac{gh_1h_2}{c^2 - gh_2}, \qquad \alpha_3 = c, \qquad \alpha_4 = \frac{gh_1c}{c^2 - gh_2}. \tag{3.13}$$

Thus the analogue of (3.6) corresponding to $c = +c_e$, is

$$h_1 L u_1 + \frac{gh_1}{c_e^2 - gh_2} h_2 L u_2 + c_e L h_1 + \frac{gh_1}{c_e^2 - gh_2} c_e L h_2 = 0, \tag{3.14}$$

where

$$L\theta \equiv \frac{\partial\theta}{\partial t} + c_e \frac{\partial\theta}{\partial x} \tag{3.15}$$

and c_e is given by (3.12). In (3.14–15) all the dependent variables are advected with speed c_e toward positive x. The analogue of (3.6) corresponding to $c = -c_e$ is obtained by reversing the sign of c_e in (3.14) and (3.15); then all the variables are advected toward negative x. Finally, the two equations corresponding to internal gravity waves are obtained by replacing c_e in (3.14–15) by $\pm c_i$. The four equations thus obtained are equivalent to the set (3.10), but unlike (3.10) each of these four equations involves propagation at a single speed.

Our numerical approximation consists of replacing the x-derivatives in each equation like (3.14) by the third-order-upwind formula corresponding to the unique propagation direction in that equation, and then solving the equations for the time-derivatives of the four independent variables. For example, in (3.14), corresponding to $c = +c_e$, (3.15) is replaced by

$$L\theta = \frac{\partial \theta}{\partial t} + c_e \vec{\theta}_x \tag{3.16}$$

while in the analogue of (3.14) corresponding to $c = -c_i$ we take

$$L\theta = \frac{\partial \theta}{\partial t} - c_i \vec{\theta}_x. \tag{3.17}$$

The algebra proves somewhat tedious, but the final result assumes a revealing form if, taking the Boussinesq limit of small density difference between the layers, we expand the c's and α_i's in powers of ε. Then, omitting terms of order ε^2 and $\varepsilon\Delta^4$, we obtain

$$\frac{\partial u_1}{\partial t} + gd_x(h_1 + h_2) = \tag{3.18a}$$

$$-\sqrt{\frac{g}{h_1 + h_2}} \, (h_1 D_x u_1 + h_2 D_x u_2) + \sqrt{g\varepsilon} \, \frac{h_1^{1/2} h_2^{3/2}}{(h_1 + h_2)^{3/2}} D_x(u_2 - u_1)$$

and three analogous equations for the time derivatives of u_2, h_1, and h_2. Here d_x and D_x are finite-difference operators defined by

$$d_x\theta \equiv \frac{1}{2}(\vec{\theta}_x + \tilde{\theta}_x) \qquad \text{and} \qquad D_x\theta \equiv \frac{1}{2}(\vec{\theta}_x - \tilde{\theta}_x). \tag{3.19}$$

Using Taylor-series expansions of gridded variables in the definitions (2.11–12), we find that

$$d_x\theta = \frac{\partial \theta}{\partial x} + O(\Delta^4) \qquad \text{and} \qquad D_x\theta = \frac{\Delta^3}{12} \frac{\partial^4 \theta}{\partial x^4} + O(\Delta^4), \tag{3.20}$$

where Δ is the grid-spacing. Thus, as expected, (3.18a) is a logical finite-difference approximation to (3.10a). The stabilizing hyperdiffusion terms in (3.18a)—the terms on the right-hand side of (3.18a)—represent the leading-order truncation error, and are analogous to the hyperdiffusion in (2.4–5).

As in Section 2, we obtain the y-direction analogues of these equations by carrying out this entire procedure in the y-direction, that is, by considering (3.10) with u_1 and u_2 replaced by v_1 and v_2, and with the x-derivatives replaced by y-derivatives. Then we collect results to obtain the finite-difference analogues of (3.9). In ready-to-code form, the full set of finite-difference equations for the non-advective part, (3.9), of the dynamics comprises (3.18a), the three equations

$$\frac{\partial u_2}{\partial t} + gd_x((1 - \varepsilon)h_1 + h_2) = -\sqrt{\frac{g}{h_1 + h_2}} \, (h_1 D_x u_1 + h_2 D_x u_2) \tag{3.18b}$$

$$+ \sqrt{g\varepsilon} \, \frac{h_1^{3/2} h_2^{1/2}}{(h_1 + h_2)^{3/2}} D_x(u_1 - u_2)$$

$$\frac{\partial h_1}{\partial t} = -h_1(d_x u_1 + d_y v_1) - \sqrt{g}\,\frac{h_1}{(h_1 + h_2)^{1/2}}\,(D_x + D_y)(h_1 + h_2)$$

$$+ \frac{\sqrt{g\varepsilon h_1 h_2}}{(h_1 + h_2)^{3/2}}\,(h_1(D_x + D_y)h_2 - h_2(D_x + D_y)h_1) \qquad (3.18c)$$

$$\frac{\partial h_2}{\partial t} = -h_2(d_x u_2 + d_y v_2) - \sqrt{g}\,\frac{h_2}{(h_1 + h_2)^{1/2}}\,(D_x + D_y)(h_1 + h_2)$$

$$+ \frac{\sqrt{g\varepsilon h_1 h_2}}{(h_1 + h_2)^{3/2}}\,(h_2(D_x + D_y)h_1 - h_1(D_x + D_y)h_2) \qquad (3.18d)$$

and two additional equations obtained by replacing u by v, d_x by d_y, and D_x by D_y in (3.18a) and (3.18b). We refer to this complete set of 6 equations as (3.18). Once again, we may add forces not involving the derivatives of dependent variables by simply adding them to the right-hand sides of (3.18). As in (2.5) the hyperdiffusion terms in (3.18) are anisotropic. However, unlike (2.5) there are no cross-diffusion terms in (3.18) or, for that matter, in the corresponding equations for (3.8).

4. One layer model with bottom topography

Returning to the single-layer case, we note that the presence of a rigid bottom boundary at vertical location $z = -H(x, y)$ generalizes the one-layer shallow-water equations to

$$\frac{\partial \mathbf{u}}{\partial t} + \mathbf{u} \cdot \nabla \mathbf{u} = -g\nabla h + g\nabla H \qquad (4.1)$$

and

$$\frac{\partial h}{\partial t} + \nabla \cdot (h\mathbf{u}) = 0. \qquad (4.2)$$

The term arising from the bottom topography enters (4.1) as a prescribed force, suggesting that this term might simply be added to the right-hand side of the one-layer analogue of (3.18). However, this "bottom force" is also a potential force which would, in the presence of frictional dissipation, eventually lead to state of rest in which the fluid layer forms a "puddle" of depth $h = H(x, y) - C$ in the region $H(x, y) > C$, where the constant C is determined by the total volume of fluid present. Unless the numerics are carefully designed to be compatible with this state of rest, the bottom topography generates large, unphysical persistent flows, even in the presence of dissipation.

To clarify these points we consider the one-dimensional, one-layer analogue of the finite-difference equations derived in Section 3, namely

$$\frac{\partial u}{\partial t} = -g d_x h - \sqrt{gh} D_x u \qquad (4.3)$$

and

$$\frac{\partial h}{\partial t} = -hd_x u - \sqrt{gh}D_x h \tag{4.4}$$

These are obtained by setting $h_1 = \varepsilon = 0$ in (3.18), and by throwing away the equations for the upper layer. Eqs. (4.3–4) are finite-difference approximations to the one-layer analogues of (3.10). The naive procedure of simply adding the term $+gd_x H$ to the right-hand side of (4.3) produces finite-difference equations that include bottom topography with the same $O(\Delta^4)$ accuracy as (4.3–4). However, the equations thus obtained are incompatible with the state of rest; the tendency of the $D_x h$-term in (4.4) to make h uniform can only be balanced by a persistent u that turns out to be of significant size in the oceanographic applications we have in mind. The better strategy is to replace (4.3) and (4.4) by

$$\frac{\partial u}{\partial t} = -gd_x(h - H) - \sqrt{gh}D_x u \tag{4.5}$$

and

$$\frac{\partial h}{\partial t} = -hd_x u - \sqrt{gh}D_x(h - H). \tag{4.6}$$

in which $H(x, y)$ also appears in the hyper-diffusion term of (4.6). Eqs. (4.5–6) have the same accuracy as (4.3–4), correctly incorporate the bottom force, and are exactly compatible with the state of rest $u = 0$, $h = H - C$. A similar trick may be applied in the two-layer case.

Both (4.5–6) and its two-layer analogue work quite well provided that neither fluid layer approaches zero thickness. However, this is an unacceptable restriction on the two-layer case. In the state of rest, the lower layer of a two-layer ocean has vanishing thickness in shallow coastal regions, where the upper layer completely fills the water column. Unfortunately, states with vanishing layer thicknesses seem incompatible with the methods proposed in Sections 2 and 3, because the equations lose their hyperbolic character as $h \to 0$. Moreover, ad hoc methods of preventing $h = 0$ (such as simply resetting h if it falls below a prescribed lower bound, or adding a bottom drag which becomes very large when the layer thickness becomes small) seem to destabilize the method. The better strategy is to modify the physics in such a way as to make the state of rest correspond to a state in which regions of vanishing layer thickness become regions of very small thickness instead.

We continue to consider the one-layer case, but, with the two-layer case as our goal, we regard the one-layer equations as the equations for the lower layer of a two-layer ocean, with the upper layer at rest. Thus the g in (4.1) is reduced gravity. Omitting the advection terms (which occur in their own separate split), (4.1) may be written as

$$\frac{\partial \mathbf{u}}{\partial t} = -\nabla\left(\frac{\delta V}{\delta h}\right) \tag{4.7}$$

where $\delta V/\delta h$ is the functional derivative of the potential energy

$$V = \int\int dx\, dy\left\{ gh\left(-H + \frac{1}{2}h\right)\right\}. \tag{4.8}$$

Inserting a term that becomes large as h becomes small, we define the modified potential energy,

$$V_m = \int\int dx\, dy\left\{ gh\left(-H + \frac{1}{2}h\right) + gP(h)\right\}. \tag{4.9}$$

where $P(h)$ is an arbitrary function with the properties that $P(h)$ is negligible when $h \gg h_0$, where h_0 is a small positive constant, and $P(h) \to \infty$ as $h \to 0$. The modified dynamics

$$\frac{\partial \mathbf{u}}{\partial t} = -\nabla\left(\frac{\delta V_m}{\delta h}\right) = -g\nabla(h - H + P'(h)) = -g(1 + P''(h))\nabla h + g\nabla H \tag{4.10}$$

has a state of rest corresponding to

$$h - H + P'(h) = const. \tag{4.11}$$

Suppose, for example, that

$$P''(h) = \left(\frac{h_0}{h}\right)^n \tag{4.12}$$

where h_0 is a positive constant, and n is a positive integer greater than 1. Then the rest state (4.11) corresponds to

$$h - \frac{1}{n-1}\frac{h_0^n}{h^{n-1}} = H(x, y) + C \tag{4.13}$$

where the constant C is determined by the total volume of fluid. Suppose this volume is such that $h = H_{max}/2$ at $H = H_{max}$, where H_{max} is the maximum of H. This corresponds to a puddle with its surface a vertical distance $H_{max}/2$ below the highest elevation attained by the rigid lower boundary at, say, $H = 0$. Refer to Figure 1. Then, assuming $h_0 \ll H_{max}$, $C \simeq -H_{max}/2$, and (4.13) becomes

$$h - \frac{1}{n-1}\frac{h_0^n}{h^{n-1}} = H(x, y) - \frac{1}{2}H_{max} \tag{4.14}$$

Within the puddle, the second term in (4.14) is negligible, and we obtain the rest state $h = H - H_{max}/2$ corresponding to the unmodified dynamics. Above the puddle, the fluid
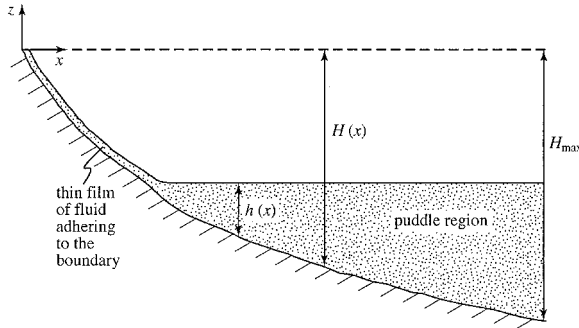
Figure 1. The state of rest (4.13) of a one-layer fluid in a deep container. In the "puddle region" the fluid surface is flat at the level corresponding to half the maximum container depth. Higher up, the fluid adheres to the boundary in a thin layer.

adheres to the solid bottom in a thin layer. In this region, the first term in (4.14) is negligible, and we obtain

$$h = \left[\frac{h_0^n}{(n-1)(\frac{1}{2}H_{\max} - H)} \right]^{1/(n-1)} \tag{4.15}$$

for the thickness of the thin layer. This layer thickness decreases with decreasing H to the minimum layer thickness,

$$\frac{h}{H_{\max}} = \left(\frac{2}{n-1}\right)^{1/(n-1)} \left(\frac{h_0}{H_{\max}}\right)^{n/(n-1)} \tag{4.16}$$

at $H = 0$. The relation (4.16) guides the choice of h_0. According to (4.16), $h \to h_0$ as $n \to \infty$.

For general $P(h)$, the modified dynamics

$$\frac{\partial u}{\partial t} + g(1 + P''(h)) \frac{\partial h}{\partial x} - g \frac{\partial H}{\partial x} = 0 \tag{4.17}$$

and

$$\frac{\partial h}{\partial t} + h \frac{\partial u}{\partial x} = 0 \tag{4.18}$$

may be written in form (3.6) as

$$\left(\frac{\partial}{\partial t} + c \frac{\partial}{\partial x}\right) u + \frac{c}{h}\left(\frac{\partial}{\partial t} + c \frac{\partial}{\partial x}\right) h - g \frac{\partial H}{\partial x} = 0 \tag{4.19a}$$

and

$$\left(\frac{\partial}{\partial t} - c\frac{\partial}{\partial x}\right)u - \frac{c}{h}\left(\frac{\partial}{\partial t} - c\frac{\partial}{\partial x}\right)h - g\frac{\partial H}{\partial x} = 0, \tag{4.19b}$$

where

$$c = \sqrt{gh(1 + P''(h))} \tag{4.20}$$

is the phase speed corresponding to the modified dynamics. When $h \gg h_0$, $c^2 \approx gh$ as in the unmodified case. However, when $h \ll h_0$, $c^2 \approx gh(h_0/h)^n$. At the minimum thickness predicted by (4.16)

$$c^2 = \frac{(n-1)}{2}gH_{\max}. \tag{4.21}$$

Thus for large n the phase speed of waves on the thin film of fluid adhering to the bottom exceeds the maximum phase speed of ordinary gravity waves, requiring the time step to be shorter than in unmodified dynamics. This is the "stiffness penalty" for an excessively "hard" $P(h)$. However, numerical experiments show that the modified dynamics work quite well with relatively small n—we shall mainly use $n = 4$—requiring little or no shortening of the time step. For $n = 4$, c exceeds $\sqrt{gH_{\max}}$ by a factor of only 1.22.

Unfortunately, the equations

$$\left(\frac{\partial u}{\partial t} + c\vec{u}_x\right) + \frac{c}{h}\left(\frac{\partial h}{\partial t} + c\vec{h}_x\right) - g\vec{H}_x = 0 \tag{4.22a}$$

and

$$\left(\frac{\partial u}{\partial t} - c\tilde{u}_x\right) - \frac{c}{h}\left(\frac{\partial h}{\partial t} - c\tilde{h}_x\right) - g\tilde{H}_x = 0 \tag{4.22b}$$

obtained by replacing the spatial derivatives in (4.19) by third-order-upwind differences are not compatible with the state of rest (4.11), because differences—unlike derivatives—do not obey the chain rule

$$\frac{c^2}{h}\frac{\partial h}{\partial x} = \frac{\partial}{\partial x}(gh + gP'(h)). \tag{4.23}$$

Therefore we must use the differential relation (4.23) *before* replacing the derivatives by finite differences. That is, instead of (4.22) we use

$$\frac{\partial u}{\partial t} + c\vec{u}_x + \frac{1}{c}\left(\frac{\partial \phi}{\partial t} + c\vec{\phi}_x\right) = 0 \tag{4.24a}$$

and

$$\frac{\partial u}{\partial t} - c\tilde{u}_x - \frac{1}{c}\left(\frac{\partial \phi}{\partial t} - c\tilde{\phi}_x\right) = 0, \tag{4.24b}$$

where

$$\phi \equiv g(h - H + P'(h)). \tag{4.25}$$

By summing and differencing (4.24), we obtain the equation for $\partial u/\partial t$ and the x-derivative contribution to the equation for $\partial\phi/\partial t$. Then, carrying out the same procedure in the y-direction, and using (4.25) to eliminate $\partial\phi/\partial t$ in favor of $\partial h/\partial t$, we finally obtain

$$\frac{\partial u}{\partial t} = -d_x\phi - cD_x u$$

$$\frac{\partial v}{\partial t} = -d_y\phi - cD_y v \tag{4.26}$$

$$\frac{\partial h}{\partial t} = -h(d_x u + d_y v) - \frac{h}{c}(D_x + D_y)\phi$$

where, once again, the finite-difference operators are defined by (3.19). Our numerical approximation consists of alternate time steps of (4.26) and the third-order-upwind approximation to

$$\frac{\partial \mathbf{u}}{\partial t} = -u\frac{\partial \mathbf{u}}{\partial x} - v\frac{\partial \mathbf{u}}{\partial y}$$

$$\frac{\partial h}{\partial t} = -u\frac{\partial h}{\partial x} - v\frac{\partial h}{\partial y} \tag{4.27}$$

These finite-difference equations are compatible with the state of rest, because the state of rest corresponds to $u = v = 0$ and $\phi = const$. Note that, although the introduction of the artificial potential $P(h)$ alters the energy of the system, it has no effect on potential vorticity conservation, because the curl of $\nabla\phi$ vanishes whether $P(h)$ is present or not.

5. Two-layer model with bottom topography

Now, using all our tricks, we derive finite-difference analogues of the two-layer shallow water equations with bottom topography. To add the topography, and to prevent either layer thickness from vanishing, we introduce the modified potential energy

$$V_m = g \int\int dx\, dy \{\rho_1 h_1(-H + h_2 + \tfrac{1}{2}h_1)$$

$$+ \rho_2 h_2(-H + \tfrac{1}{2}h_2) + \rho_1 P(h_1) + \rho_2 P(h_2)\} \tag{5.1}$$

The corresponding dynamics is

$$\frac{\partial \mathbf{u}_i}{\partial t} + \mathbf{u}_i \cdot \nabla \mathbf{u}_i = -\nabla \phi_i \tag{5.2a}$$

and

$$\frac{\partial h_i}{\partial t} + \nabla \cdot (h_i \mathbf{u}_i) = 0, \tag{5.2b}$$

where

$$\phi_1 \equiv \frac{1}{\rho_1} \frac{\delta V_m}{\delta h_1} = g(h_1 + h_2 - H + P'(h_1)) \tag{5.3a}$$

and

$$\phi_2 \equiv \frac{1}{\rho_2} \frac{\delta V_m}{\delta h_2} = g((1 - \varepsilon)h_1 + (h_2 - H) + P'(h_2)). \tag{5.3b}$$

As before, $i = 1$ (2) refers to the top (bottom) layer, and $\varepsilon = (\rho_2 - \rho_1)/\rho_2$ is the relative density difference between the layers. As in Section 3, we solve (5.2) by the method of operator splitting. In the first split, we step (3.8) forward one time-step using third-order-upwind differences based on the direction of the fluid velocity, $\mathbf{u}_1$ or $\mathbf{u}_2$. In the second split we step

$$\frac{\partial \mathbf{u}_i}{\partial t} = -\nabla \phi_i \tag{5.4}$$

and

$$\frac{\partial h_i}{\partial t} = -h_i \nabla \cdot \mathbf{u}_i. \tag{5.5}$$

in the forms

$$\frac{\partial \phi_1}{\partial t} = -c_1^2 \nabla \cdot \mathbf{u}_1 - gh_2 \nabla \cdot \mathbf{u}_2 \tag{5.6a}$$

and

$$\frac{\partial \phi_2}{\partial t} = -c_2^2 \nabla \cdot \mathbf{u}_2 - (1 - \varepsilon)gh_1 \nabla \cdot \mathbf{u}_1, \tag{5.6b}$$

where

$$c_1^2 \equiv gh_1(1 + P''(h_1)) \qquad \text{and} \qquad c_2^2 \equiv gh_2(1 + P''(h_2)). \tag{5.7}$$

Our use of the variables ϕ_1 and ϕ_2 in place of h_1 and h_2 anticipates the requirement that the finite-difference equations be compatible with the state of rest.

Again we proceed by rewriting the one-dimensional form of (5.4) and (5.6) in the general form (3.6). This leads to

$$\alpha_1 Lu_1 + \alpha_2 Lu_2 + \alpha_3 L\phi_1 + \alpha_4 L\phi_2 = 0 \tag{5.8}$$

where

$$L = \left(\frac{\partial}{\partial t} + c\frac{\partial}{\partial x}\right) \tag{5.9}$$

and

$$\alpha_1 = (1 - \varepsilon)gh_1, \quad \alpha_2 = c^2 - c_1^2, \quad \alpha_3 = (1 - \varepsilon)gh_1/c, \quad \alpha_4 = (c^2 - c_1^2)/c. \tag{5.10}$$

The wave speed c takes the four values $c = \pm c_e, \pm c_i$, where

$$c_e^2, c_i^2 = \frac{c_1^2 + c_2^2}{2} \pm \frac{1}{2}\{(c_1^2 - c_2^2)^2 + 4(1 - \varepsilon)gh_1gh_2\}^{1/2} \tag{5.11}$$

and c_e (c_i), corresponding to the plus (minus) sign in (5.11), is the speed of external (internal) waves in the modified dynamics. Thus (5.8) represents four equations. Once again, we obtain finite-difference equations by replacing the x-derivative in (5.9) by a third-order-upwind difference. That is,

$$L\theta = \left(\frac{\partial\theta}{\partial t} + c\vec{\theta}_x\right) \tag{5.12}$$

when $c = +c_e$ or $c = +c_i$, and

$$L\theta = \left(\frac{\partial\theta}{\partial t} + c\overleftarrow{\theta}_x\right) \tag{5.13}$$

when $c = -c_e$ or $c = -c_i$. We solve the four equations represented by (5.8) for the time-derivatives of u_1, u_2, ϕ_1, and ϕ_2, obtaining the finite-difference analogues of (5.4), and of (5.6) without the y-derivative terms. Then we repeat the whole procedure in the y-direction, obtaining the time-derivatives of v_1 and v_2 and the y-derivative terms in (5.6). Finally, we convert the time-derivatives of ϕ_1 and ϕ_2 into time-derivatives of h_1 and h_2, using the definitions (5.3). The resulting equations represent the generalization of the equations derived in Section 3 to include nonuniform fluid depth $H(x, y)$ and the effects of $P(h_1)$ and $P(h_2)$. When H is constant, $P(h) \equiv 0$, and ε is small, these equations reduce to (3.18). By construction, these finite-difference equations are consistent with the state of rest, in which ϕ_1 and ϕ_2 are uniform.

In the next section we present numerical solutions that demonstrate the accuracy and stability of our algorithms. First we give the few remaining numerical details. The use of operator-splitting demands that the time-stepping algorithm be "self-contained," that is, that it not refer to conditions before the alternate step. A simple method having this

property is second-order Runge-Kutta, also called the "mid-point method." If the equation is $dy/dt = F(y)$, the algorithm is

$$y_{n+1/2} = y_n + \frac{1}{2}\Delta t F(y_n)$$

$$y_{n+1} = y_n + \Delta t F(y_{n+1/2})$$

(5.14)

where Δt is the time step, and y_n the value of y at $t = n\Delta t$. All the solutions described in Section 6 use (5.14) for both members of the split.

Except where noted, our solutions use no-normal-flow at solid boundaries as the only boundary condition. Near the boundaries, third-order upwind formulae like (2.11–12) may require modification. For example, at first interior gridpoints, we replace third-order upwind differences by first-order upwind differences where needed. This replacement slightly reduces the accuracy of the resulting finite-difference equations near the boundaries, but we observe no spurious behavior near boundaries in any of our solutions.

6. Numerical examples

The best test of any numerical algorithm is comparison with exact analytical solutions. Unfortunately, most nontrivial exact solutions of the shallow water equations are one-dimensional. However, one of these provides an excellent test of our method for preventing negative layer thickness. Carrier and Greenspan (1958) give an exact solution of the one-layer shallow-water equations corresponding to a standing wave on a uniformly sloping beach. With $g = 1$ and $H = x$, their solution of (4.1–2) is given implicitly by

$$u = -\frac{A}{4\sqrt{h}} J_1(4\sqrt{h}) \cos(2u - 2t)$$

(6.1)

and

$$x = \frac{1}{2}u^2 + h + \frac{A}{4} J_0(4\sqrt{h}) \sin(2u - 2t)$$

(6.2)

where J_0 and J_1 are Bessel functions. Given any $h \geq 0$ and t, (6.1) uniquely determines u provided that $|A| < 1$. Then x is given by (6.2). In this way we determine $u(x, t)$ and $h(x, t)$. As $x \to \infty$ (6.1–2) approach the solution

$$u \approx -\frac{A}{4\sqrt{x}} J_1(4\sqrt{x}) \cos(2t)$$

(6.3a)

and

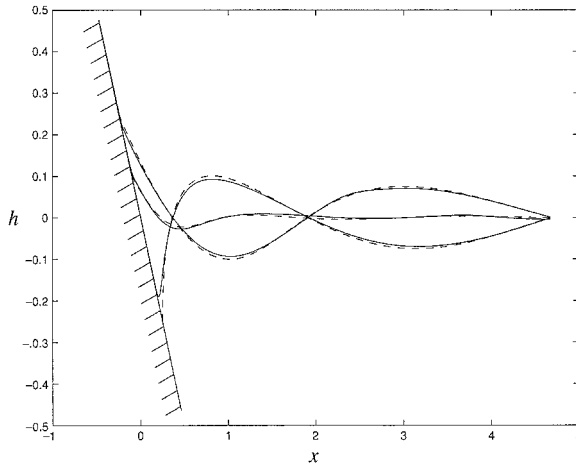$$\eta \equiv h - x \approx \frac{A}{4} J_0(4\sqrt{x}) \sin(2t)$$

(6.3b)

Figure 2. Dashed curve: the wave height in the analytical solution (6.1–2) corresponding to an inviscid, shallow-water, standing wave with amplitude $A = 1$ on a sloping beach, at three times in the wave cycle. Solid curve: the corresponding numerical solution with the small explicit viscosity $\nu = \Delta$. The straight line, representing the solid bottom, has a 45-degree slope.

of the linearized equations, where η is the surface elevation above its rest state. Thus (6.1–2) correspond to a wavetrain reflected from a sloping beach. When $|A| > 1$, the wave forms a bore, and the solution of (6.1–2) is multi-valued.

Figure 2 shows the analytical solution (6.1–2) for the maximum amplitude $A = 1$, and the corresponding numerical solution of (4.26–27) at three times in the wave cycle. The numerical solution includes the artificial potential $P(h)$ with $h_0 = 0.01$ and $n = 4$. The numerical solution also includes a small explicit viscosity of the momentum-conserving form

$$\frac{\partial u}{\partial t} + \ldots = \frac{\nu}{h} \frac{\partial}{\partial x} \left(h \frac{\partial u}{\partial x} \right) \tag{6.4}$$

with viscosity coefficient $\nu = \Delta$ where Δ is the grid-spacing. (About 500 grid spaces cover the fluid domain in Fig. 2.) The smallness of this explicit viscosity can be gauged by the good agreement between the analytical and numerical solutions; the analytical solution is for inviscid flow.

Figure 3 compares the same analytical solution to the numerical solution with no explicit viscosity ($\nu = 0$). In this case, the only stabilizing diffusion is that provided by the implicit hyperdiffusive truncation error associated with third-order upwinding. When $\nu = 0$, the numerical solution contains small, spurious pulses generated at the beach as the wave recedes from its maximum incursion; four of these pulses can be seen in Figure 3. The
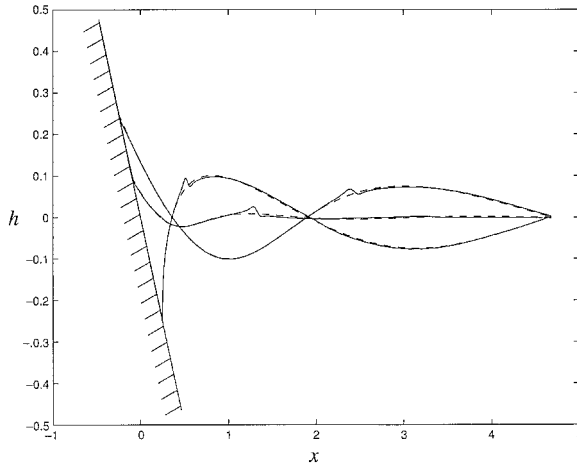
Figure 3. The same as Figure 2, except that the numerical solutions contains no viscosity or explicit dissipation of any kind. Four spurious pulses are visible in the numerical solution.

pulses, which exit the computational domain on the right side of the figure,[4] evidently arise from an interaction between the wave and the thin film of water clinging to the beach. This film is invisible on the scale of Figure 3. The pulses represent errors in the numerical solution, but their smallness, and the fact that they disappear with the addition of a small explicit viscosity, suggest that this error is insignificant. In fact, the generally good behavior of the numerical model in the limit of no explicit viscosity suggests that our algorithm is robust.

The numerical solutions seem relatively insensitive to the choice of exponent n in the definition (4.12) of the artificial potential. I found no significant difference in the solutions corresponding to $n = 4$ and $n = 10$. However, the coefficient h_0, which controls the depth of the fluid film, cannot be too small for the chosen spatial resolution. The criterion seems to be that, in the equation (4.13) for the state of rest, the balance of terms cannot change over a distance much smaller than the grid distance Δ. Let $x = 0$ correspond to the transition point. Then in the vicinity of $x = 0$, (4.13) takes the form

$$y - \frac{1}{(n-1)} y^{1-n} = \frac{sx}{h_0}, \qquad (6.5)$$

where $y \equiv h/h_0$ and s is the bottom slope. From (6.5) it is clear that the criterion referred to above requires $h_0 > s\Delta$. With the current values $s = 1$ and $\Delta = 0.01$, this corresponds to $h_0 > 0.009$. Figure 4 shows the state of rest computed from (4.13) using Newton's method and the value $h_0 = 0.01$ used in the numerical solutions of Figures 2 and 3. The putative

---

4. As the boundary condition on the numerical solution, we prescribe the velocity u predicted by the solution (6.3) of the linearized equations.
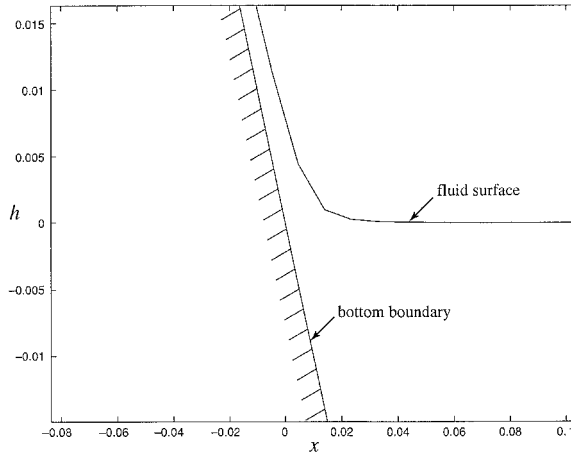
Figure 4. A close-up view of the "shoreline" in the state of rest corresponding to Figures 2 and 3. With $h_0 = 0.01$ and a beach slope of $s = 1$, the transition between deep water and the fluid film adhering to the beach occurs over a distance comparable to the grid-spacing.

stability criterion is clearly being approached. Solutions with $h_0 = 10^{-3}$ show significant numerical noise, and when $h_0 = 10^{-4}$ the state of rest is itself unstable.

Other solutions, especially those containing bores, require an explicit viscosity. One of these corresponds to the removal of a dam separating quiescent reservoirs with different surface heights. The "weak" form of the analytical solution is given by Stoker (1957, pp. 333–37). It consists of a fan moving into the deeper reservoir and a bore propagating in the opposite direction. Again we set $g = 1$. The initial conditions are $h = 1$ to the left ($x < 0$) of the dam at $x = 0$, and $h = h_R$ on $x > 0$. Figure 5 shows the analytical and numerical solutions for the case $h_R = 0.5$ at a sequence of times after the dam disappears. Once again, the analytical solution corresponds to inviscid flow, while the numerical solution contains a small explicit viscosity with $\nu = 0.1\Delta$. The two solutions agree closely.

Figure 6 compares the same analytical solution to the numerical solution with no explicit viscosity ($\nu = 0$). In this case, the numerical solution contains large, spurious spikes at the location of the bore, and it underestimates the speed of the bore. These defects are even more evident in the case $h_R = 0.1$ (not shown), in which the bore is stronger. The error in the bore speed is clearly associated with the fact that our implicit hyperdiffusion—the D_x and D_y terms in (4.26)—manifestly violates momentum conservation, whereas classical shock-fitting theory reminds us that the correct bore speed depends upon conservation laws. If strong bores are present in the solution, then we must, as in Figure 5, include an explicit, momentum-conserving viscosity, but it is reassuring to note that, even without such a viscosity, our algorithm is stable and in qualitative agreement with the exact solution.

The question of whether to include explicit dissipation in numerical algorithms—and what kind of dissipation to choose—is actually quite subtle. Phenomena like bores or the
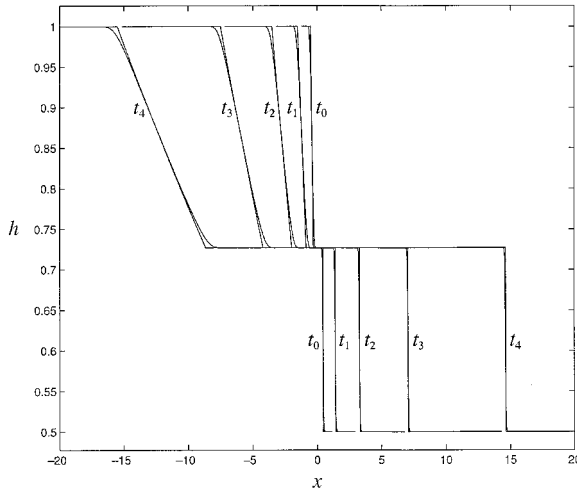
Figure 5. The analytical and numerical solutions for surface height $h(x, t)$ at a sequence of times after the breakage of a dam separating a reservoir with $h = 1$ on $x < 0$ from a reservoir with $h = 0.5$ on $x > 0$. The analytical solution is the "weak solution" (with viscous regions unresolved) and therefore has discontinuous derivatives. The numerical solution contains an explicit viscosity of form (6.4) with $v = 0.1\Delta$, where Δ is the grid-spacing.

use of no-slip boundary conditions clearly demand an explicit viscosity, but one strongly suspects that unnecessarily large viscosities are often introduced to stabilize poorly designed algorithms. In large-scale geophysical fluid dynamics strong bores are rare, the
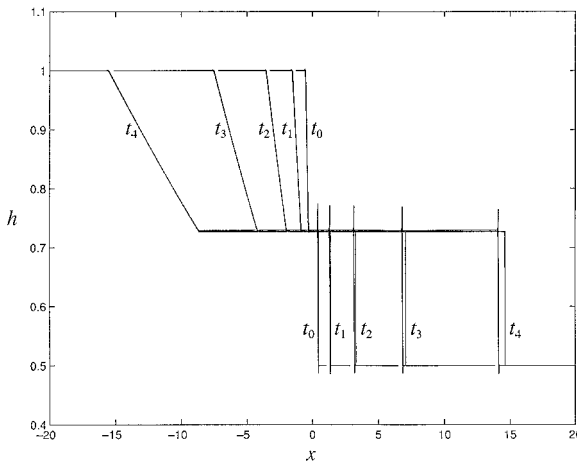

Figure 6. The same as Figure 5 except that the numerical solution has no explicit viscosity ($v = 0$). The numerical solution contains spurious spikes at the location of the bore, and it underestimates the speed of the bore.

need for no-slip boundary conditions is debatable, and the primary role of dissipation—explicit or implicit—is to remove the enstrophy that would otherwise pile up at the shortest resolved lengthscale. For this the hyperdiffusive truncation error associated with third-order upwinding seems ideal and may be sufficient by itself to absorb the enstrophy cascade. After all, despite their being anisotropic, the implicit hyperdiffusion terms in (3.18) resemble the explicit biharmonic diffusion commonly used in "large-eddy simulations." Griffies and Hallberg (2000) advocate the use of a biharmonic dissipation with a coefficient proportional to the local strain rate, in somewhat the same way that the coefficients of the D-terms in (3.18) depend on the local values of h_1 and h_2. Thus we may regard (3.18) as an algorithm with fourth-order-accurate differences, and a sub-grid-scale viscosity that just happens to take the form of the D-terms in (3.18), or as an algorithm with third-order-accurate differences, in which the D-terms represent the leading-order truncation error.

I greatly prefer the latter viewpoint. No matter what difference scheme one chooses, truncation error will be present. If this truncation error can serve as an effective sub-gridscale viscosity, then so much the better. Numerical experiments suggest that the truncation error associated with third-order upwinding is often sufficient by itself to prevent the accumulation of enstrophy on the grid-scale. For example, the numerical simulations of geostrophic turbulence depicted in Salmon (1998) use no sub-grid-scale dissipation except that implicit in the third-order upwinding of potential-vorticity advection.[5]

Now we turn to two-dimensional solutions of the one- and two-layer equations in a 4000×8000 km ocean with its southern boundary at the equator. The ocean is driven by a 2-gyre wind stress, of maximum amplitude 2 dyn cm^{-2}, with westerlies and trade winds, as shown on the left of Figure 7. In the one-layer case (Fig. 7, right), the g in (3.18) is reduced gravity, $g = 0.002g_t$, where $g_t \equiv 9.8$ m sec^{-2}, and the equations represent a single layer of moving fluid above a deeper layer that remains everywhere at rest, even where it lies exposed to the wind. In the 2-layer case (Figs. 8–12), the reduced gravity is $\varepsilon g = 0.002g_t$, while the external gravity $g = 0.05g_t$ is taken to be 20 times smaller than its true value g_t. This permits the time step to be about 4.5 times larger than if $g = g_t$. Variations in the free surface elevation are then 20 times larger than those observed, but they are smaller than the variations in the depth of the interface between layers by the factor $\varepsilon = 0.04$. In all solutions, each moving layer absorbs a fraction of the wind momentum equal to the fraction, occupied by that layer, of the upper 100 m of the water column. Thus, in water less than 100 m deep, a portion of the wind stress is transmitted directly to the solid bottom. In this way we account for vertical momentum transport by small-scale processes not contained in the model, and we prevent the huge accelerations that could develop when a finite momentum flux acts on a region of infinitesimal depth. For the artificial potential we use $n = 4$ and $h_0 = 20$ m. With this value of h_0, the minimum
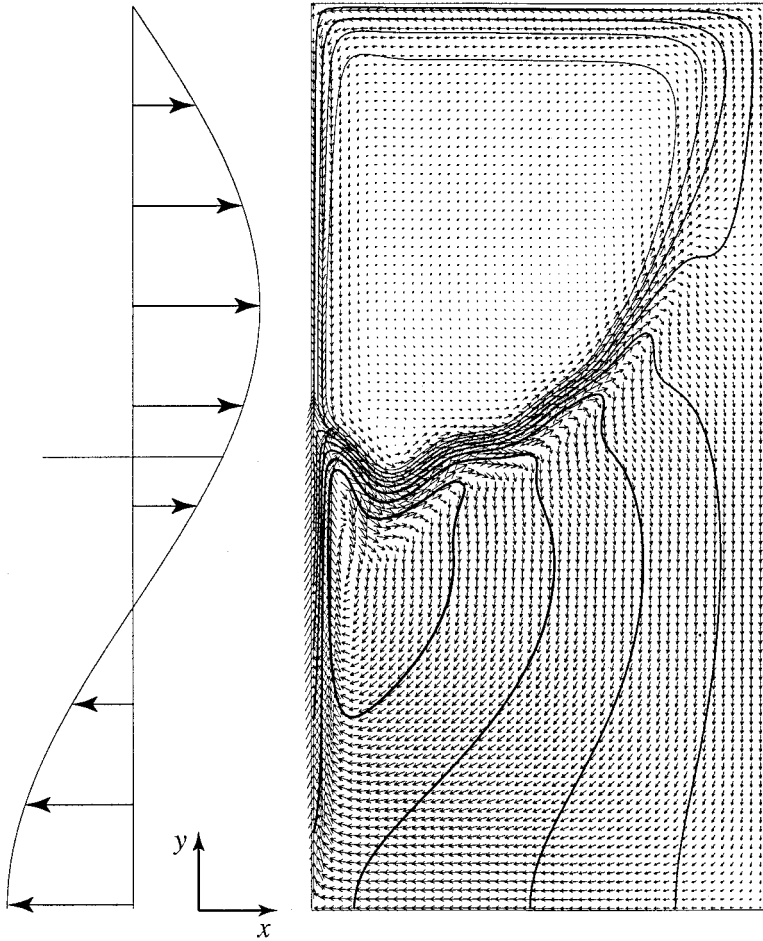
---

5. See Figures 4.9, 6.2 and 6.3 in Salmon (1998).

Figure 7. Left: the eastward wind stress, of maximum amplitude 2 dyn cm^{-2}, used in all solutions. Westerlies occur over the northernmost 2/3 of a 4000×8000 km ocean. The southern boundary coincides with the equator. Right: the layer thickness (contours) and transport $h\mathbf{u}$ (arrows) in the single-layer (reduced-gravity) solution. The lower layer is assumed to be at rest, even in the large subpolar region in which it outcrops at the ocean surface. Darker contours correspond to larger values. Maximum layer thickness, 435 m. Arrows are proportional to the square root of the transport. Maximum velocity, 163.6 km day^{-1}. Rms velocity, 14.2 km day^{-1}.

layer thickness is about 10 m. Much smaller h_0 (and smaller minimum thickness) is possible, but only if the spatial resolution is increased beyond the 100×200 gridpoints used in most of our solutions.

   None of our two-dimensional solutions uses an explicit sub-gridscale viscosity. In fact, the only explicit dissipation is Rayleigh friction of the form

$$\frac{\partial \mathbf{u}}{\partial t} = \cdots - \lambda \mathbf{u}. \tag{6.6}$$

In all of our solutions, the decay coefficient λ corresponds to a Stommel boundary layer thickness $\sqrt{\lambda/\beta}$ of 60.6 km. In the cases with 100×200 resolution, this represents a boundary layer only 1.5 grid distances thick. All the solutions were integrated at least 18 years from an initial state of rest. To set the initial condition, we use Newton's method to obtain accurate solutions of (4.13) and the analogous two-layer equations, $\phi_1 = C_1$, $\phi_2 = C_2$, for the initial layer thicknesses. This is necessary because ϕ_1, ϕ_2 depend very sensitively on the layer thicknesses when the latter are small. However, after the initial time we use the chain rule to convert time-derivatives of ϕ_1, ϕ_2 to time-derivatives of h_1, h_2, and there is thus no further need to solve transcendental equations.

   The 1-layer (reduced-gravity) solution of Figure 7 resembles the planetary geostrophic (i.e. non-inertial), analytical solutions of Parsons (1969) and Veronis (1973), except for the meanders in the separated western boundary current. These meanders clearly result from the presence of inertia in shallow-water dynamics.

   Figure 8 shows the corresponding two-layer solution in an ocean with a flat bottom at a depth of 4 km. The volume of upper-layer water is about the same as in the one-layer solution of Figure 7. The two-layer solution resembles the flat-bottom, planetary geostrophic, analytical solution of Kamenkovich and Reznik (1972). Because the lower layer is everywhere much thicker than the upper layer, the upper-layer circulation in Figure 8 closely resembles that in Figure 7. To the extent that inertia is negligible, the vertically integrated transport in a flat-bottom ocean must agree with Stommel's classic theory. In particular, the separated western boundary current must be cancelled by an eastward current directly beneath it. The lower-layer flow in Figure 8 does contain such a countercurrent, but the cancellation is inexact; the total transport of both layers (Fig. 11, left) shows a large, inertial correction to Sverdrup flow near the location of the separated boundary current. Because the two-layer model admits baroclinic instability, the meanders in this current are much larger than those in Figure 7.

   Figure 9 shows a two-layer solution with bottom topography. This solution differs from the solution in Figure 8 only in the presence of continental shelves and slopes along the western, northern, and eastern boundary. The shapes and widths of these slopes can be gauged from Figure 12.[6] The presence of coastal topography significantly changes the circulation of both layers. In the upper layer (Fig. 9, left) the Gulf Stream follows the coastline to the latitude of zero wind-stress. There it detaches from the coastline, but it does not move far offshore. Instead the current follows the isobaths along the continental slope before smoothly heading out to sea at the mid-latitude. Everywhere north of the initial separation, the flow along the coastline itself is southward. This contrasts sharply with the single-layer and flat-bottom cases of Figures 7 and 8, where the flow along the coastline is

---

6. The equatorial boundary remains a vertical wall, corresponding to mirror symmetry of the flow across the equator. Recall that our only boundary condition is no-normal-flow.
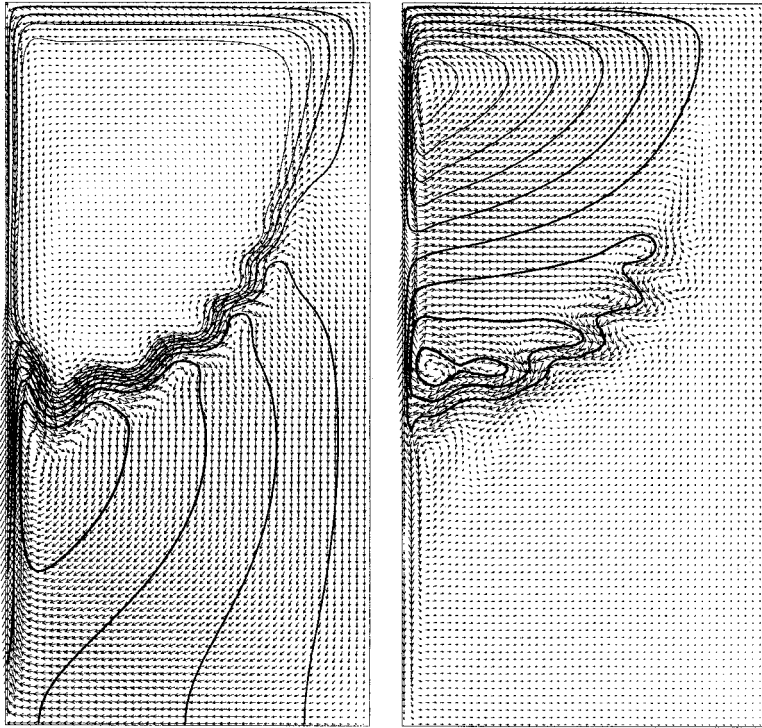
Figure 8. The circulation in a two-layer ocean with a uniform depth of 4 km and the same wind stress as in Figure 7. Left: the upper-layer thickness (contours) and transport (arrows). Right: the lower-layer dynamic topography (contours) and transport (arrows). Maximum upper-layer thickness, 442 m. Maximum (rms) upper-layer velocity, 169.9 (15.5) km day^{-1}. Lower layer, 9.55 (0.72) km day^{-1}.

northward until well past the latitude of Gulf Stream separation, which itself appears to be delayed. That is, in Figures 7 and 8, the Gulf Stream overshoots its latitude of separation. However, it is the lower-layer flow that differs most dramatically between Figures 8 and 9. In the solution with topography, the meanders beneath the separated western boundary current are much stronger, and there is a huge, deep southward flow at the foot of the western continental slope. This southward flow is distinct from that which occurs beneath the northward upper-layer flow nearer the coast at low latitudes. The latter flow is present in both Figures 8 and 9. Figures 9 and 10 do not depict the flow in the physically insignificant regions with layer depths less than h_0, but the flow in these regions seems smooth and well-behaved.

Both bottom topography and inertia cause the vertically integrated flow to depart from Sverdrup flow. Thus it is not surprising that the vertically integrated transport in the solution with topography (Fig. 11, right) differs even more than the transport in the flat-bottom solution (Fig. 11, left) from classical theory.
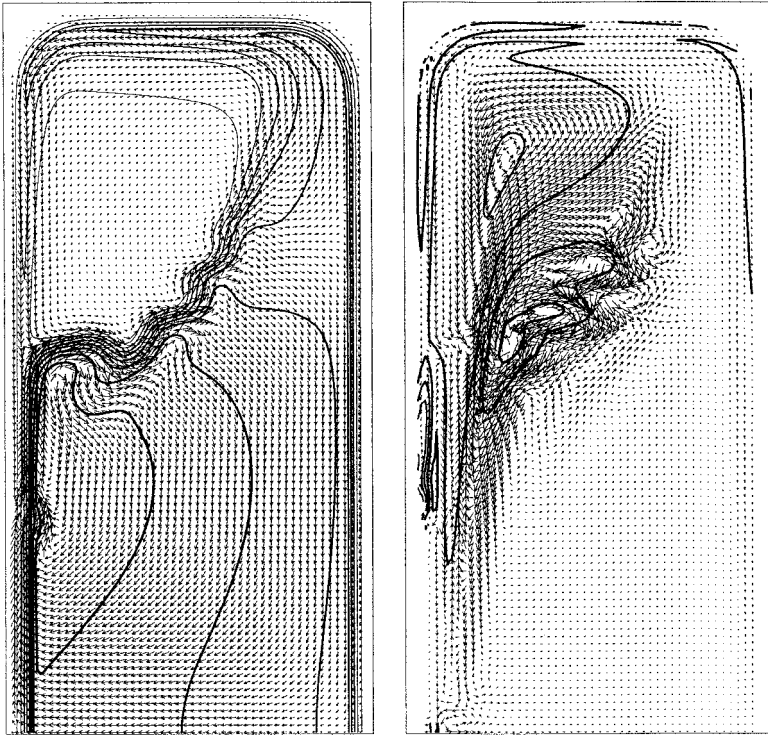
Figure 9. The circulation in a two-layer ocean with a maximum depth of 4 km and continental shelves and slopes at the western, northern and eastern boundaries. The scale of the slopes can be gauged from Figure 12. Left: the upper-layer thickness (maximum 467 m) and transport. Maximum (rms) velocity, 304.5 (19.9) km day^{-1}. Right: the lower-layer dynamic topography and transport. Maximum (rms) velocity, 29.3 (2.07) km day^{-1}. Regions with layer thickness less than h_0 are not depicted.

The lower-layer flow in Figure 9 resembles previous analytical and numerical studies of homogeneous (i.e. one-layer) flow over western continental slopes. See, for example, Salmon (1992), Becker and Salmon (1997), and references therein. For example, the deflection of lower-layer flow features in Figure 9 toward the southwest corner of the ocean is clearly associated with the convergence of f/H-lines at that point. Unfortunately, despite the remarkable contribution of Ford (2000), who considered a piecewise homogeneous ocean with horizontal density jumps, we seem to be rather far from a complete theory of stratified western boundary currents over coastal topography.

Figures 8 and 9 show a notable lack of eddy activity in regions far from the separated boundary currents. Figure 10 shows the circulation 3.5 years after doubling the resolution in the solution shown in Figure 9. The smaller grid spacing of 20 km better resolves the internal deformation radius, and it means that the implicit biharmonic diffusion is 8 times smaller than in Figure 9. (Recall that the diffusion coefficient varies as Δ^3.) The current
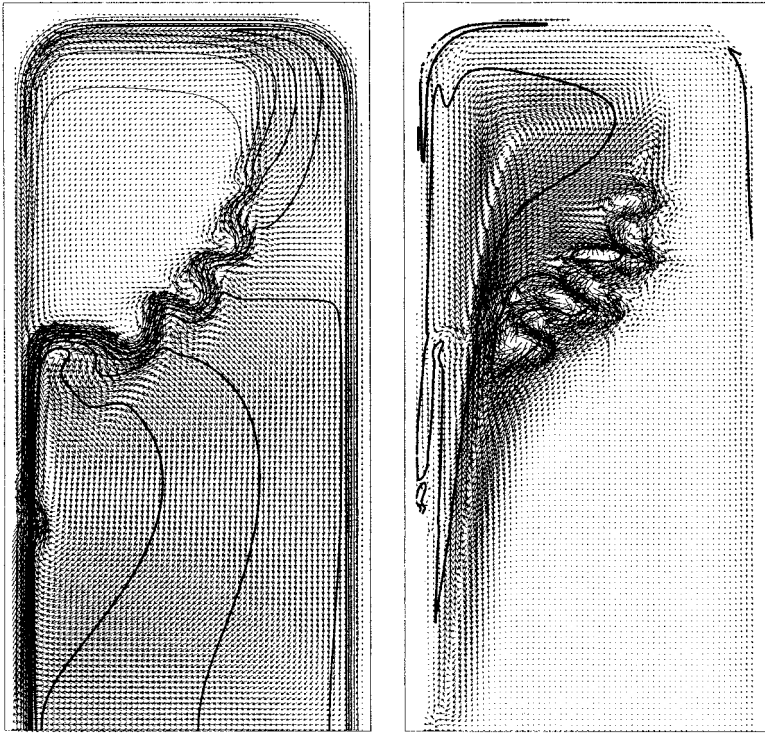
Figure 10. The same as Figure 9, but 3.5 years after doubling the resolution from 100×200 to 200×400. The lower-layer maximum (rms) velocity increases to 34.0 (2.47) km day^{-1} as the deep meanders in the separated western boundary current increase in amplitude. The upper-layer velocity increases by a smaller proportion, to 325.7 (maximum) and 20.4 km day^{-1} (rms).

meanders are stronger in the better resolved solution, and a close inspection of Figure 10 reveals a higher level of eddy activity in the deep subtropical ocean.

Finally, Figure 12 shows three sections across the high-resolution solution of Figure 10. These sections show again how the method represents surface- and bottom outcrops with thin layers. At the latitude of Figure 12a, the Gulf Stream, judged by its transport, has already separated from the coastline, but the upper layer still has its maximum depth on the continental slope. At the latitude of Figure 12b, the wind stress curl is positive. Hence the upper layer shoals to the west, and the separated western boundary current is rather diffuse. Figure 12c is a north-south section along the base of the western continental slope. It shows the Gulf Stream wall and the much more diffuse eastward current along the northern boundary.

7. Discussion

We solve the two-layer shallow water equations by transforming the equations into characteristic form and by applying third-order-upwind differences to each equation. A
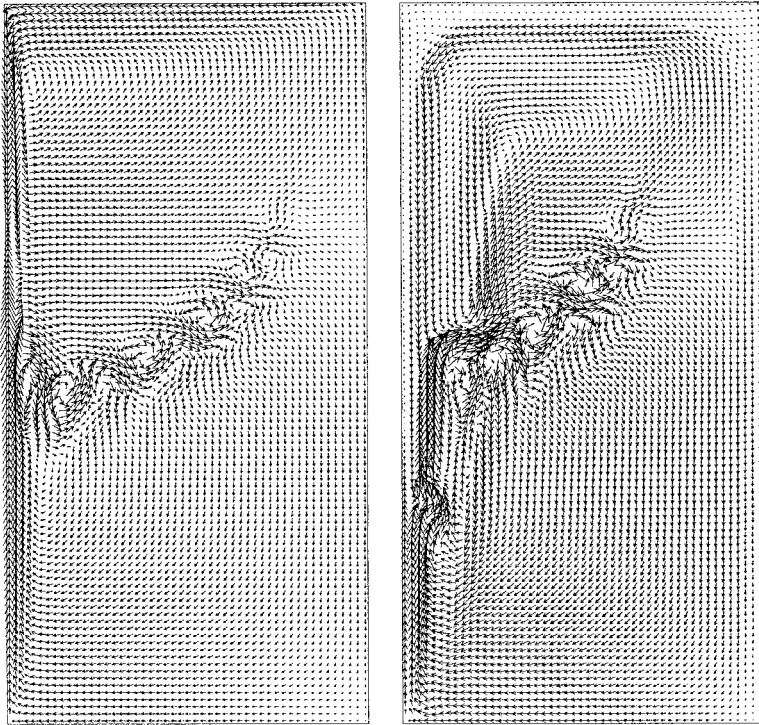
Figure 11. The total transport of both layers in the two-layer solutions with a flat bottom (left), and with continental shelves and slopes (right). The transport on the left differs from classical (Sverdrup-Stommel) theory only because inertia is present. The transport on the right differs from classical theory because of both inertia and bottom topography.

complete set of characteristics exists only if the equations are hyperbolic. However, the shallow water equations are hyperbolic only in the one-dimensional case, and then only if neither layer depth vanishes. Even in one space dimension, the characteristics of the two-layer system require extensive computations.

To circumvent these difficulties, we divide the time step into two parts: a strictly advective part, and a part consisting of everything else. Each of these parts is further divided into its two directional components. Each directional component represents a hyperbolic system *provided* we introduce an artificial potential to prevent the layer thicknesses from vanishing. Separating each hyperbolic system into its individual wave components, we apply the third-order-upwind method, with the upwind direction based on the direction of wave propagation. Third-order upwind is almost the simplest non-oscillatory scheme that might have been used—only first-order upwind is simpler, and it is much too dissipative to be practical—but this simplicity is virtually indispensable in oceanographic applications requiring millions of time steps. Although I have not seen this particular combination of techniques applied to the shallow water equations, the artificial
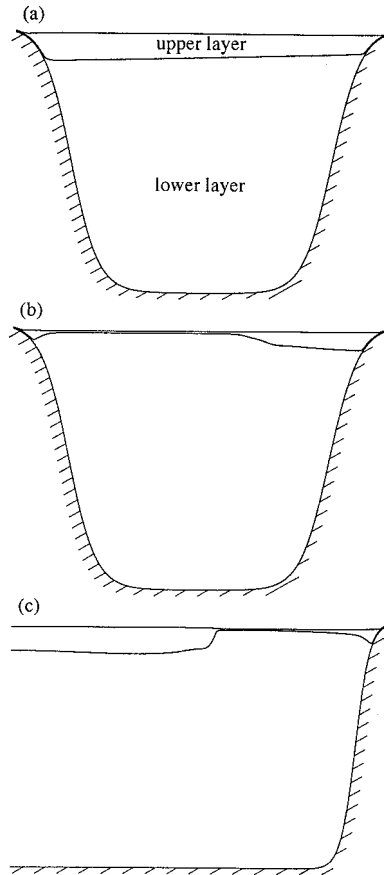
Figure 12. Sections at (a) $y = 3000$ km, across the subtropical gyre; (b) $y = 6000$ km, across the subpolar gyre; and (c) $x = 1000$ km, along the foot of the western continental slope, in the high-resolution experiment depicted in Figure 10.

potential is the only really novel component of our method. Compared to high-order Riemann schemes with flux or slope limiters, our method is formally more accurate, probably less dissipative, and certainly more efficient. However, because we do not exactly conserve momentum and mass, bores move at the wrong speed unless we add explicit, momentum-conserving viscosity. For oceanographic applications, our scheme is an alternative to the method developed by Hallberg and Rhines (1996).

All of the calculations described in Section 6 use the full strategy summarized in the preceding paragraph. As explained in Section 2, the one-layer equations do not require operator-splitting into advective and non-advective parts. However, numerical experiments showed no significant difference between one-layer solutions computed with the operator-splitting algorithm and solutions computed with the algorithm of Section 2.

Our method easily generalizes to an arbitrary number of fluid layers. However, the calculation of the wave speeds becomes more costly as the number of layers increases. For example, a 3-layer model requires the solution of a cubic polynomial for c^2 at every gridpoint and time.

For oceanographic applications, our scheme does not require the use of an explicit, sub-gridscale viscosity. The implicit hyperdiffusion associated with third-order upwind effectively absorbs the enstrophy cascade to small scales. This raises the question of whether our algorithm is really superior to a centered, fourth-order difference scheme with an *arbitrary* explicit biharmonic momentum diffusion. That is, in (say) the one-layer case, does the form of the dissipation terms on the right-hand sides of (3.18) have special significance? To partly answer this question, I compared solutions of (3.18) with and without the D-terms in the continuity equations (3.18c) and (3.18d). The motivation for this is that, in arbitrarily prescribing an eddy viscosity, one would not normally think of adding hyperdiffusion terms to the shallow-water continuity equations. In both one- and two-layer cases, it was found that solutions without the D-terms in the continuity equations gradually developed grid-scale oscillations that eventually ruined the solutions. These oscillations had large divergence (compared to, say, their vorticity). A similar, divergence-mode noise occurred in a series of two-layer shallow-water models constructed by the author over the past two years, using algorithms based upon the lattice Boltzmann method as well as more conventional methods using finite differences and finite elements. In all cases except those reported in this paper, it was found that the divergence-mode noise could only be controlled by adding a dissipation so large that interesting physical features disappeared.

Bühler (1998) attributes this misbehavior of the shallow water equations to the tendency of the equations to form bores. To avoid it, he proposes replacing the pressure gradient force ∇h by a force proportional to $h^{-3}\nabla h$, which uniquely averts bore formation. Bühler's suggestion is practical for cases of nearly uniform h, but it is inapplicable to oceanic studies in which $h \to 0$.

An alternative strategy, also briefly entertained by Bühler, is to introduce nonhydrostatic (i.e. Boussinesq) corrections to shallow-water physics. Nonhydrostatic effects introduce wave dispersion, which interferes with the formation of bores. Coriolis force also causes dispersion, but Coriolis effects are often insignificant at the smallest resolved lengthscales. The typically coarse spatial resolution of oceanographic models renders nonhydrostatic effects similarly unimportant. However, numerous investigations suggest that the deliberate exaggeration of nonhydrostatic effects by, for example, inserting a coefficient greater than unity—but not so great as to upset leading-order hydrostatic balance—in front of the Dw/Dt-term in the vertical-momentum equation, leads to better-behaved numerics. See, for example, Browning *et al.* (1990), Mahadevan *et al.* (1996), Huck *et al.* (1999), and Salmon (1999). The nonhydrostatic equations are also nonhyperbolic, so the methods of this paper would not apply; on the other hand, they might not then be needed. This alternative strategy deserves further investigation.

This paper is dedicated to the memory of my friend and colleague Rupert Ford, who attacked the problem of western boundary currents over topography with inspirational skill, tenacity, and cheerfulness.

REFERENCES

Becker, J. M. and R. Salmon. 1997. Eddy formation on a continental slope. J. Mar. Res., *55,* 181–200.

Browning, G. L., W. R. Holland, H.-O. Kreiss and S. J. Worley. 1990. An accurate hyperbolic system for approximately hydrostatic and incompressible oceanographic flows. Dyn. Atmos. Oceans, *14,* 303–332.

Bühler, O. 1998. A shallow-water model that prevents nonlinear steepening of gravity waves. J. Atmos. Sci., *55,* 2884–2891.

Carrier, G. F. and H. P. Greenspan. 1958. Water waves of finite amplitude on a sloping beach. J. Fluid Mech., *4,* 97–109.

Ford, R. 2000. A baroclinic western boundary current over a continental slope. J. Mar. Res., *58,* 327–373.

Godlewski, E. and P.-A. Raviart. 1996. Numerical Approximation of Hyperbolic Systems of Conservation Laws, Springer-Verlag, 509 pp.

Griffies, S. M. and R. W. Hallberg. 2000. Biharmonic friction with a Smagorinsky-like viscosity for use in large-scale eddy-permitting ocean models. Mon. Wea. Rev., *128,* 2935–2946.

Hallberg, R. and P. B. Rhines. 1996. Buoyancy-driven circulation in an ocean basin with isopycnals intersecting the sloping boundary. J. Phys. Oceanogr., *26,* 913–940.

Hecht, M. W., W. R. Holland and P. J. Rasch. 1995. Upwind-weighted advection schemes for ocean tracer transport: An evaluation in a passive tracer context. J. Geophys. Res., *100,* C10, 763–778.

Huck, T., A. J. Weaver and A. Colin de Verdiere. 1999. On the influence of the parameterization of lateral boundary layers on the thermocline circulation in coarse-resolution ocean models. J. Mar. Res., *57,* 387–426.

Kamenkovich, V. M. and G. M. Reznik. 1972. A contribution to the theory of stationary wind-driven currents in a two-layer liquid. Atmos. Ocean. Phys., *8,* 238–245.

Kurganov, A. and E. Tadmor. 2000. New high-resolution central schemes for nonlinear conservation laws and convection-diffusion equations. J. Comp. Phys., *160,* 241–282.

Lawrence, G. A. 1990. On the hydraulics of Boussinesq and non-Boussinesq two-layer flows. J. Fluid Mech., *215,* 457–480.

Leonard, B. P. 1979. A stable and accurate convective modelling procedure based on quadratic upstream interpolation. Comp. Meth. Appl. Mech. Eng., *19,* 59–98.

—— 1984. Third-order upwinding as a rational basis for computational fluid dynamics, *in* Computational Techniques and Applications: CTAC-83, J. Noye and C. Fletcher, eds., 106–120.

—— 1991. The ULTIMATE conservative difference scheme applied to unsteady one-dimensional advection. Comp. Meth. Appl. Mech. Eng., *88,* 17–74.

LeVeque, R. J. 1992. Numerical methods for conservation laws, Birkhäuser Verlag, 214 pp.

Mahadevan, A., J. Oliger and R. Street. 1996. A nonhydrostatic model. Part I: Well-posedness and scaling. J. Phys. Oceanogr., *26,* 1868–1880.

Parsons, A. T. 1969. A two-layer model of Gulf Stream separation. J. Fluid Mech., *39,* 511–528.

Salmon, R. 1992. A two-layer Gulf Stream over a continental slope. J. Mar. Res., *50,* 341–365.

—— 1998. Lectures on Geophysical Fluid Dynamics, Oxford University Press, 378 pp.

—— 1999. Lattice Boltzmann solutions of the three-dimensional planetary geostrophic equations. J. Mar. Res., *57,* 847–884.

Stoker, J. J. 1957. Water waves, Wiley-Interscience, 567 pp.

Stone, J. M. and M. L. Norman. 1992. Zeus-2d: A radiation magnetohydrodynamics code for astrophysical flows in two space dimensions. I. The hydrodynamic algorithms and tests. Astrophys. J. Suppl., *80,* 753–790.

Veronis, G. 1973. Model of world ocean circulation. Part I. J. Mar. Res., *31,* 228–288.

Vreugdenhil, C. B. 1994. Numerical methods for shallow-water flow, Kluwer Academic Publisher, 261 pp.

Whitham, G. B. 1974. Linear and nonlinear waves. John Wiley and Sons, 628 pp.